ABUAD Journal of Engineering Research and Development (AJERD)
ISSN (online): 2645-2685; ISSN (print): 2756-6811

Volume 8, Issue 3, 189-211

Alternative Framework for Generator Coherency Analysis and Controlled-Islanding for Grids with High Penetration Levels of Inverter-Based Renewables

Mbey VINCENT, Akintunde Samson ALAYANDE, Sunday ADETONA, Adeola BALOGUN

Department of Electrical/Electronic Engineering University of Lagos, Akoka, Yaba, Lagos-Nigeria
mbeyvincent@gmail.com/aalayande@unilag.edu.ng/sadetona@unilag.edu.ng/obalogun@unilag.edu.ng

Corresponding Author mbeyvincent@gmail.com, +2348162386046
Received: 28/08/2025
Revised: 24/10/2025
Accepted: 31/10/2025
Available online: 12/11/2025

Abstract: *The increasing integration of inverter-based renewable energy sources has significantly altered power system dynamics and reduced inertia. Identifying coherent generators in such low-inertia systems remains a major challenge due to the dynamic influence of renewable variability. Previous research considered rotor angles and rotor speed separately. Also, the fast dynamics introduced by inverter-based renewables on power system variables make it pertinent to simultaneously consider rotor angles and rotor speed dynamics for coherency detection. Moreover, many authors have established coherency detection schemes but few have validated their methods with controlled islanding making their methods less practical for the modern grid with renewables. This paper proposes a unified coherency detection framework that combines rotor angles and rotor speeds within a dynamic state vector to capture both oscillatory and speed dynamics. An adaptive coherency threshold is computed from the geometric mean of the Euclidean distances between rotor state time series of distinct generators, allowing the threshold to adjust to changing system conditions. The framework is validated on the IEEE 30-bus system and applied to controlled islanding based on network topology and generation–load balance. The proposed framework achieved smooth dynamic responses following disturbances. These results confirm the method's suitability for real-time application and its potential to improve resilience in modern power systems with high renewable integration.*

Keywords: *Rotor Angle, Rotor Speed, Coherent Generators, Controlled Island, Generation-Load Imbalance*

1. INTRODUCTION

Adding more components to a power grid increases system complexity and coupling, which can introduce new oscillatory modes, reduce inertia, and make the grid more prone to dynamic instability unless coordinated control measures are implemented. Moreover, the presence of diverse control strategies and time constants across different devices can lead to poorly damped inter-area oscillations and slower synchronization among generators and, consequently, a voltage collapse [1]. Contingencies such as major line outage, generator trip, or cascading fault can cause the interconnected power grid to quickly lose synchronism, leading to widespread instability or even a total blackout [2].

Controlled islanding serves as a last-resort corrective action designed to preserve system integrity by intentionally separating the grid into smaller, self-sustained islands before instability spreads[3]. By strategically disconnecting certain transmission lines, controlled islanding confines disturbances within localized areas, maintaining frequency and voltage stability in the remaining islands. This approach ensures that critical loads continue to receive power and facilitates faster system restoration after the disturbance[4]. Hence, controlled islanding is essential for enhancing the resilience of modern power systems [5].

Identifying coherent generators plays a crucial role in the design of effective controlled islanding schemes. During severe system disturbances, power systems can lose synchronism, leading to widespread instability or cascading outages. For islanding to preserve stability, generators within each island must operate in synchrony—hence the importance of identifying groups of coherent generators that exhibit similar dynamic behaviour [6]. By grouping coherent generators into the same island, inter-area oscillations are minimized, and internal dynamic stability is maintained[7]. Consequently, coherency detection provides the dynamic foundation upon which topological and operational criteria for island boundaries are built [8]. This consequently helps in ensuring that each formed island remains stable, balanced, and capable of independent operation after separation [9].

Several similarity measures can be implemented on rotor angles and rotor speed, after which affinity propagation-based clustering analysis can be implemented on the similarity measures to form coherent groups [10]. Maíra R. Monteiroa et al. [11] deployed the energy function approach on generator frequency data to determine coherent areas with wind-based and solar-based Renewable Energy Sources (RES), after which it was revealed that the solar-based RES had a significant impact on the coherency analysis scheme when compared to wind-based RES. Hasan BANNA et al. [12] implemented the Dynamic Time Warp Algorithm (DTW), which is an algorithm for analyzing similarities in time series data, on

synchrophasor data to determine coherent generators. This method proved effective with some with delays, data losses, and a certain level of noise in processing synchrophasor data. Panayiotis Demetriou et al. [13] showed that the power system is modeled as a graph, and the intraclass correlation coefficients are estimated from rotor angle data to group coherent machines. However, the scheme requires that several intended coherent groups be specified. Mohammad Reza Aghamohammadi et al. [14] applied Pearson's correlation coefficients to process estimated rotor angle data and machine speed of generators for coherency identification. The implemented schemes proved to be independent of changes in network structure. On the other hand, identifying coherent generators can be achieved by using the cosine of the angles between speed deviation vectors of two generators as a similarity measure to establish the generator coherency. Cosine values between speed deviations of 2 generators tending towards 1 indicate coherence [15]. Shengyuan Liu et al.[16] implemented coherency identification schemes for a renewable energy-integrated power system through the use of Fuzzy C-Mean (FCM) clustering on simulated frequency data following a system disturbance. The FCM was employed to solve for 2 coherent groups, after which an Adjustable Robust Optimization Programming (AROP) was employed to find optimal islanding solutions. Although optimal solutions of power balance were found for the islands, the islanding solution was not tested. Wei Yawei et al. [17] implemented k-Harmonic means clustering to identify coherency generators for a case study with significant Photovoltaic (PV) penetration. Yadav Ravi et al. [18] employed clustering on frequency data through the Discrete Cosine Stockwell Transform (DCST). Key features from the DCST are then used to identify generators with similar dynamics. Sevda Jafarzadeh et al. [19] and Fredrik Raak et al. [20] used Koopman Mode Analysis (KMA) on PMU rotor angle data and rotor speed, respectively, to quickly identify coherent generator groups. These groups are revealed by the Koopman Modes (KMs), which capture the spatial patterns of synchronous swing. This real-time identification is directly applied to designing defensive islanding schemes to prevent system instability from spreading. Radial Basis Function Neural Network (RBFNN) can be employed to train and process PMU signals from generator terminals to determine coherent generator groups under random load fluctuations [21]. Moreover, Abhilash Kumar Gupta et al. [22] combined rotor angle data with PCA and a Feed Forward Neural Network (FFNN) to form independent groups of coherent generators, demonstrating that the FFNN required less computational effort than the RBFNN. Isnaadh et al. [23], deployed a Long Short-Term Memory (LSTM) network that was optimized using simulated rotor angle data. The LSTM model achieved high accuracy across several performance metrics and remained robust under conditions of limited input data and computational constraints. Overall, the LSTM outperformed traditional machine learning techniques, including Artificial Neural Networks (ANN), in identifying coherent generators. The slow coherency method determines the number of coherent groups by analyzing the system's slowest oscillation modes that appear before a disturbance occurs using Equations (1) and (2) [24], and [25].

$$\Delta\ddot{\delta} = [M^{-1}K]\Delta\delta \tag{1}$$

Where:
δ is rotor angle in radians
$\Delta\delta$ is the deviation of rotor angles from the steady state
K is the synchronizing torque coefficient Matrix
H is a diagonal matrix of generator inertia
ω_0 is the grid's nominal frequency
$M = \frac{2H}{\omega_0}$, is the diagonal matrix of generators scaled inertia
E_i' is the transient phasor EMF of the i_{th} generator
B_{ij} are the real entries of the systems Y_{BUS}
G_{ij} are the imaginary entries of the systems Y_{BUS}
n is the number of generators

$$K_{ij} = \begin{cases} -|E_i'||E_j'|\{B_{ij}\,cos(\delta_i - \delta_j) - G_{ij}\,sin(\delta_i - \delta_j)\},\ i \neq j \\ -\sum_{l=1,l\neq i}^{n} K_{il}\ ,\ i = j \end{cases} \tag{2}$$

Following the linearization of the power grid, the modes are obtained as the eigenvalues of ($\mathrm{M}^{-1}\mathrm{K}$). Thus, for a grid of the nth order, i.e., 'n' number of generators implies there will be n modes and n corresponding eigenvectors. The slowest modes are then selected with the number of slowest modes, the number of coherent groups of generators [26], [27] and [28]. Thus, coherency is achieved before system disturbance by modal characterization of the eigenvectors corresponding to the slow modes [29], [30], and [31]. However, the slow coherency approach is limited in the sense that its results are independent of the location of the fault and size of system disturbance [32] and [33]. Conversely, Zhu Yizhe et al. [34] establish an adaptive slow coherency identification algorithm by considering various operating conditions and disturbance magnitude. The approach combines principles from slow coherency and nonlinear dynamical system theory, extending beyond the limitations of traditional linearized methods to adaptively determine coherent generator groups

Numerous methods have for identifying coherent generators have been highlighted. However, clustering methods require that the number of coherent groups be specified before they can be implemented. Moreover, the rise in renewable energy penetration levels tends to introduce a strong influence of fast dynamics on the power system variables, along with the depleted inertia of the power grid. Hence, Honglei Song et al. [35] and Mariotto et. al [36] considered only rotor angles and rotor speed, respectively, for coherence detection, which may no longer suffice. Furthermore, the depleted inertia and fast dynamics introduced by high penetration levels of inverter-based resources render the slow coherency approach no longer suitable for the modern power grid. Clustering-based techniques do not offer any way to determine an optimal number of coherent groups for a practical grid. Thus, high numbers of coherent groupings for clustering-based methods may lead to an unnecessarily large number of islands, which may be more challenging to control. Many coherency detection methods have not been validated through the implementations of controlled islanding [37–41], and [42].

The aim of this paper, therefore, is to contribute a unified framework for identifying coherent generators and to validate the established coherency framework through controlled islanding. This unified framework considers the simultaneous impact of rotor angles and rotor speed dynamics on coherency, making it well-suited for grids with high penetration of inverter-based renewables. The unified framework is a simple and effective method for coherence analysis, which focuses on capturing deeper measures of generator dynamics and does not require a priori assumptions, as other methods that are based on clustering techniques do.

The rest of the paper is as follows: Section 2 entails a Methodology for the detection of coherent generators and, along with a controlled-islanding scheme; Section 3 details Results and Discussions of the proposed coherency detection and controlled-islanding scheme; and finally, Section 4 captures the Conclusion.

2. METHODOLOGY

2.1 Coherency Detection Scheme:

This section details the unified framework for coherence detection. Honglei Song et al. [35]showed that 2 generators a and b have rotor angles. $\delta^a(t)$ and $\delta^b(t)$ observed over a time interval $[t_1, t_2]$ following a system disturbance, can be said to have a similar rotor angle trajectory if their similarity measure is $\left|\delta^a(t) - \delta^b(t)\right|_{[t_1, t_2]}$ falls below a small value (ε) using Equation (3) :

$$\left|\delta^a(t) - \delta^b(t)\right|_{[t_1, t_2]} \leq \varepsilon \tag{3}$$

Mariotto et. al [36] also show that 2 generators having rotor speeds, $\omega^i(t)$ and $\omega^j(t)$ observed over a time interval $[t_1, t_2]$can be said to have a similar rotor speed trajectory if their similarity measure $\left|\omega^a(t) - \omega^b(t)\right|_{[t_1, t_2]}$ Falls below a specified coherency threshold (ζ) using Equation (4):

$$\left|\omega^a(t) - \omega^b(t)\right|_{[t_1, t_2]} \leq \zeta \tag{4}$$

Where:

ε and ζ are small values for establishing coherence

$[t_1, t_2]$ is the time interval during which the rotor angles and rotor speeds are collected for coherency analysis post disturbances

. Honglei Song et al. [35] and Mariotto et. al [36] did not consider the simultaneous impact of rotor angles (δ) and rotor speeds(ω) on detecting coherent groups of generators.

The rotor angle and rotor speed trajectory for the i^{th} generator, G^i between t1 & t2, following extreme system disturbances will be represented by the Equation(5).

$$G^i = \begin{bmatrix} \delta_1^i & \omega_1^i \\ \delta_2^i & \omega_2^i \\ \vdots & \vdots \\ \delta_n^i & \omega_n^i \end{bmatrix} \tag{5}$$

We therefore form a dynamic vector from the rotor angle and the rotor speed trajectory of G^i . Thus, the formulated dynamic vector of $G^i$is represented using Equation (6) as:

$$G^i = [\delta^i + j\omega^i] \tag{6}$$

Where n is the number of sampling points in the captured synchronized time series data in the rotor angle and rotor speed

The Euclidean distance is chosen to serve as a similarity measure for the formulated dynamic vector of any 2 generators, as summed up in the complex Equation (7). Thus, $G^a \nabla G^b$ becomes a dynamic vector that captures rotor angle and rotor speed dynamics :

$$G^a \nabla G^b = \left[\delta^{a,b} + j\omega^{a,b}\right] \quad (7)$$

Where $\delta^{a,b}$ and $\omega^{a,b}$ are the rotor angles and rotor speed Euclidean distances between the dynamic vectors of generators a & b from Equations (8) and (9);

$$\delta^{a,b} = \sum_{k=1}^{n} \left|\delta_k^a - \delta_k^b\right| \quad (8)$$

$$\omega^{a,b} = \sum_{k=1}^{n} \left|\omega_k^a - \omega_k^b\right| \quad (9)$$

With t1 as the starting time for the rotor angle time series data and t2 as the ending time for the collected rotor angle time series data. Usually, $\delta^i(t)$ & $\omega^j(t)$ are collected between t1 & t2 during system disturbance.

Thus, for a hypothetical power grid with 4 generators G^1, G^2, G^3, G^4 The grids coherency matrix (C) can be represented as shown in Equation (10):

$$C = \begin{bmatrix} G^1 \nabla G^1 & G^1 \nabla G^2 & G^1 \nabla G^3 & G^1 \nabla G^4 \\ G^2 \nabla G^1 & G^2 \nabla G^2 & G^2 \nabla G^3 & G^2 \nabla G^4 \\ G^3 \nabla G^1 & G^3 \nabla G^2 & G^3 \nabla G^3 & G^3 \nabla G^4 \\ G^4 \nabla G^1 & G^4 \nabla G^2 & G^4 \nabla G^3 & G^4 \nabla G^4 \end{bmatrix} \quad (10)$$

The entries of the grid's coherency matrix (C) are further normalized by Equation(11):

$$C_{norm} = \frac{1}{Max(C) - Min(C)} \times C \quad (11)$$

Thus, generators a and b are coherent if Equation(12) holds:

$$|G^a \nabla G^b|_{norm} < \gamma(t) \quad (12)$$

Where $\gamma(t)$ is an adaptive coherency threshold value

It is clear that the grid's normalized coherency matrix.C_{norm} is symmetrical because the off-diagonal elements having interchanged indices represent the same coherency measure between the same generators, with their diagonal elements being zero.
Let 'd' represent the total number of distinct entries in the normalized coherency matrix. C_{norm}. Thus, for a hypothetical 4-generator system, the coherency matrix will contain 6 distinct entries.
We define an adaptive coherency threshold $\gamma(t)$ using Equation (13) as the geometric mean of all pairwise distinct Euclidean distances in C_{norm}:

$$\boldsymbol{\gamma(t) = \left(\prod_{m=1} |G^a \nabla G^b|_{norm}\right)^{\frac{1}{d}}}, \quad (13)$$

Therefore, every 'distinct' pair of generators a and b in C_{norm} i.e. $|G^a \nabla G^b|_{norm} < \gamma(t)$ having one generator in common are placed in the same coherent group, thus establishing coherency for the proposed method. The adaptive coherency threshold $\gamma(t)$ is to be calculated as the geometric mean of all the distinct pairs of Euclidean distance of the formulated dynamic vector for generators a and b. Assuming the following results in Table 1 are obtained. The first column consists of the normalized Euclidean distance between the rotor angles of a and b. Column 2 represents the normalized Euclidean distance between the rotor speeds of generators a and b. Column 3 represents the magnitude of the formulated dynamic vector. Columns with headers 'a' and 'b' are the numerical identities of the 4 generators in the hypothetical power grid. The sixth column captures the result of comparing the magnitude of the formulated dynamic vector to the formulated and calculated coherency adaptive threshold $\gamma(t)$. Thus, generators a and b are coherent with each other if the magnitude of $|G^a \nabla G^b|_{norm}$ is less than the adaptive coherency threshold.

Table 1: Coherency results from distinct pair of generators from the hypothetical 4-generator system

$\delta_{norm}^{a,b}$	$\omega_{norm}^{a,b}$	$\lvert G^i \nabla G^j \rvert_{norm}$	a	b	$\lvert G^a \nabla G^b \rvert_{norm} < \gamma(t)$
$\delta^{2,1}$	$\omega^{2,1}$	$\lvert G^2 \nabla G^1 \rvert_{norm}$	2		FALSE!
$\delta^{3,1}$	$\omega^{3,1}$	$\lvert G^3 \nabla G^1 \rvert_{norm}$	3		FALSE!
$\delta^{3,2}$	$\omega^{3,2}$	$\lvert G^3 \nabla G^2 \rvert_{norm}$	3		TRUE!
$\delta^{4,1}$	$\omega^{4,1}$	$\lvert G^4 \nabla G^1 \rvert_{norm}$	4		FALSE!
$\delta^{4,2}$	$\omega^{4,2}$	$\lvert G^4 \nabla G^2 \rvert_{norm}$	4		TRUE
$\delta^{4,3}$	$\omega^{4,3}$	$\lvert G^4 \nabla G^3 \rvert_{norm}$	4		TRUE!

The first entry of Table 1 shows that the first entry, which is a pair: generators 2 and 1, i.e., (G^2 and G^1) are not coherent with each other and therefore should not be placed in the same coherent group. The 2nd entry also shows that the pair, generator 3 and 1 (G^3 and G^1) are not coherent and don't belong to the same group. The 3rd entry shows that generators 3 and 2, i.e., (G^3 and G^2) are coherent and belong in the same coherent group. Also, the 4th entry shows that generator 4 and 2, i.e., (G^4 and G^2) are coherent and belong in the same coherent group. The 5th entry of Table 3 shows that G^4& G^3 are coherent with each other and, as such, should be placed in the same coherent group. We therefore list the coherent pairs:
Coherent pair 1: (G^3 and G^2)
Coherent pair 2: (G^4 and G^2)
We examine all the coherent pairs that have a generator in common and place them in the same coherent group, thus in this case, (G^2, G^3 and G^4) belong in the same group because the generators 3 and 4 both have G^2 in common.
However, the generator G^1, cannot be found to be coherent with any other generator. Thus $G^1$is placed in its own coherent group. Therefore, the aggregation of coherent pairs results in 2 distinct coherent groups

Group1: G^2, G^3, & G^4
Group 2: G^1

In this way, the unified framework establishes coherent groups without requiring an initial number of groupings unlike the traditional clustering methods do.

2.2 Controlled-Islanding

Implementing the formation of controlled islands entails subdividing a power system into smaller parts by opening specific branches on the power grid, thereby dividing the power grid into smaller portions having a coherent group as its energy source. This is done following a coherence analysis to terminate the spread of system disturbances [43] and [44]. It is crucial that the coherent group on an island adequately energize the load buses. This is achieved by minimizing the imbalance between the energy sources, in this case, the coherent generators within the proposed island and the load buses [45], [46]. For this study, controlled islanding will be implemented after coherency detection is established using Equation (14). Thus, the term $\sum_i^m P_{Gi}$ represents the total MW generated in a coherent group and $\sum_j^n P_{lj}$ represents the total load MW from all the load buses allocated to the coherent groups based on their proximity to the generators and topological constraints

Thus, for every island formed:
minimize $\sum_i^m P_{Gi} - \sum_j^n P_{lj} \geq 0$ (14)

Where;
m is the number of generators on an island
n is the number of load buses on an island
P_{Gi} is the MW generated by the i^{th} generator on an island
P_{li} is the MW load demand on the j^{th} bus on an island

The time series data of rotor angles and rotor speeds are then collected between t1 and t2, which is then exported to MATLAB for coherency analysis. The identified coherent groups are then used in conjunction with topological constraints, as well as generation-load imbalance minimization, to establish tie-lines to be opened for a controlled island. A second simulation is then initiated, identical to the first (location and time of 3-phase bolted faults), with which the established tie-lines for controlled islanding are then opened, after which the impact of the coherency scheme and controlled island on the power system variables is observed. Consequently, the coherency detection and controlled islanding methodology can be summarized as follows;

i. Simulate a 3-phase bolted fault on a transmission line of the case study in Powerworld simulator to create a system disturbance on power system variables.

ii. Capture rotor angle and rotor speed time series data between t1 and t2 post disturbance.
iii. Stop simulation
iv. Export rotor angle and rotor speed time series data from Powerworld simulator into MATLAB
v. Formulate dynamic vector from captured rotor angles and rotor speed
vi. Compute adaptive coherency threshold
vii. Compute coherent pairs based on the formulated dynamic vectors and adaptive coherency threshold.
viii. Aggregate each coherent pair having one generator in common into a coherent group.
ix. Place other generators that don't belong to any coherent pair in their own separate coherent group.
x. Calculate the total generation in each coherent group
xi. Allocate load buses to coherent groups based on topology and minimal generation-load imbalance using Equation (14)
xii. Identify transmission lines tying the established groups of generators and load buses, i.e, islands. These tie-lines are to be opened to form the controlled islands, with each island being energized by coherent generators.
xiii. Re-run the simulation and implement the 3-phase bolted fault as at the beginning in Powerworld simulator.
xiv. Open the identified tie-lines from MATLAB at a time t3 beyond t2 to form controlled-islands
xv. Evaluate power system variables after the opening of tie-lines

2.3 Model for Inverter-Based Renewable

The DER_A (Distributed Energy Resource – Aggregate) model is a standard dynamic model developed by the Western Electricity Coordinating Council (WECC) to represent the aggregate behaviour of inverter-based distributed energy resources (DERs), such as solar PV and battery systems, at the transmission level. It provides a simplified but comprehensive framework to study the dynamic response of large populations of DERs to grid disturbances. An illustration of the DER_A model is shown in Figure 1, which illustrates the various capabilities of the DER_A model [47]. The model is capable of performing proportional voltage, real power control, active power control, power factor control, frequency control, and post-fault recovery [48].

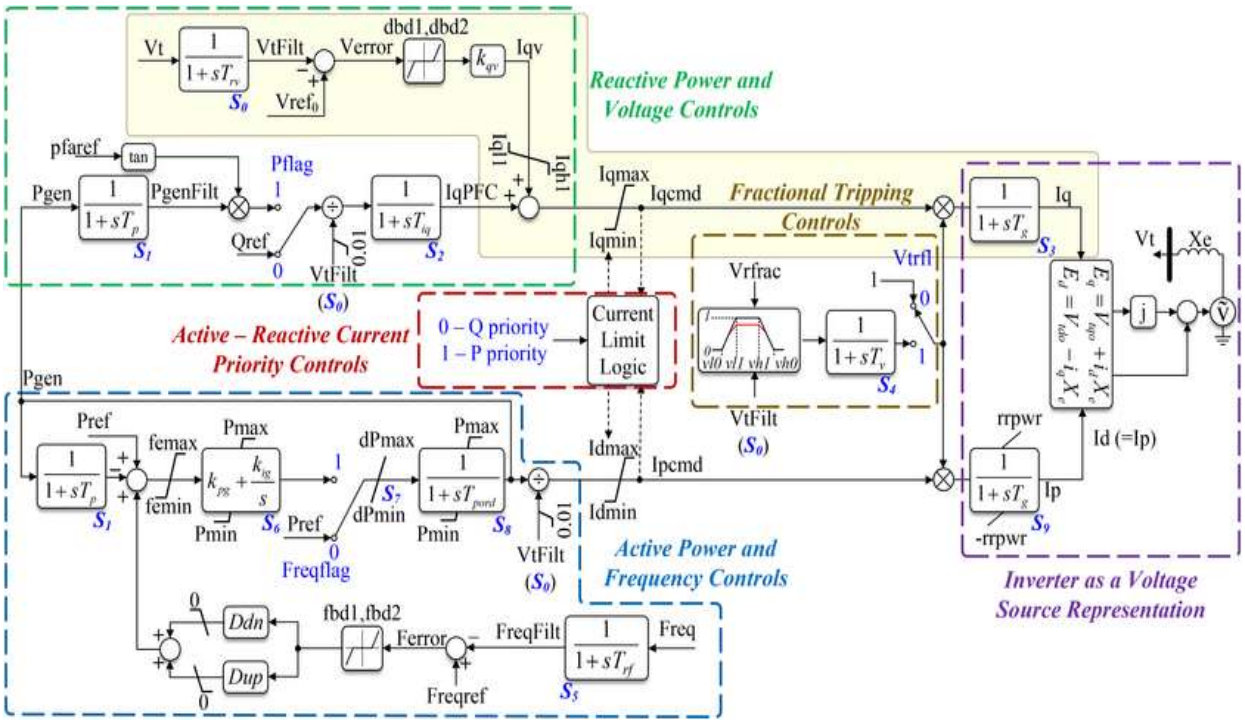

Figure 1: Schematic diagram of the DER_A model [48]

The numerous parameters of the DER_A model are parameterized based on IEEE category II-2018 data, which specifies connection standards for distributed resources [49]. The parameterization of the DER_A model is shown in Table 2.

2.4 Performance Evaluation

The performance of the implemented coherency detection and controlled islanding scheme is judged based on its impact on the power system variables, namely: system bus voltages, rotor speeds of generators, and rotor angles of generators. Thus, a properly executed grouping of coherent generators and controlled islanding will evidently stabilize the stated power system variables. Disturbances on the stated power system variables are created in the system by the implementation of 3-phase bolded fault on a transmissions line

Table 2: Parameterization of the DER_A model based on IEEE category II-2018 data

Parameter	Description	Default Parameter	Chosen Parameter
Trv	transducer time constant for voltage measurement	0.02	0.02
dbd1	lower voltage deadband	-99	-0.05
dbd2	upper voltage deadband	99	0.05
Kqv	proportional voltage control gain	0	5
vref0	Vref0: voltage reference set-point (pu)	0	0
Tp	transducer time constant (seconds)	0.02	0.02
Tiq	Q control time constant (seconds)	0.02	0.02
Ddn	down-side frequency control droop gain	20	20
Dup	up-side frequency control droop gain	20	0
fbdb1	lower frequency control deadband	-0.0006	-0.0006
fbdb2	upper frequency control deadband	0.0006	0.0006
Femax	frequency control maximum error	99	99
Femin	femin: frequency control minimum error	-99	-99
Pmax	Maximum power (pu)	1	1
Pmin	Minimum power (pu)	0	0
Dpmax	Power ramp rate up	99	99
Dpmin	Power ramp rate down	-99	-99
Tpord	Tpord: Power order time constant (seconds)	5	5
Imax	Imax: Maximum converter current (pu)	1.2	1.2
Vfrac	fraction of device that recovers after voltage comes back to within vl1 < V < vh1	1	0
Fltrp	frequency break-point for low frequency cut-out of the inverter (Hertz)	56.5	56.5
Fhtrp	frequency break-point for high frequency cut-out of the inverter (Hertz)	62	62
Tfl	frequency break-point for low frequency cut-out timer (seconds) (highly recommend that Tfl > Trf)	300	300
Tfh	frequency break-point for high frequency cut-out timer (seconds) (highly recommend that Tfh > Trf)	300	300
Tg	Current control time constant	0.02	0.02
Rrpwr	Power rise ramp rate following a fault >= 0 (pu/s	2	2
Tv	Tv: time constant on the output of the voltage cut-ou	0.02	0.02
Kpg	active power control proportional gain	0.1	0.1
Kig	active power control integral gain	10	10
Xe	Generator effective reactive (pu) > 0	0.25	0.25
Vpr	voltage below which frequency tripping is disabled (pu)	0.3	0.3
iqh1	Maximum limit of reactive current injection, p.u.	1	1
iql1	Minimum limit of reactive current injection, p.u.	-1	-1
Pfflag	0 implies constant reactive power (Q) control, 1 implies constant power factor control	1	1
Frqflag	0 implies frequency control disabled; 1 implies frequency control enabled	1	1
Pqflag	PQFlag: 0 means Q priority; 1 means P priority for current limit (any number which is not 0 is treated as 1)	1	1
Typeflag	0 means the DER_A model is a storage device and 1 means the DER_A model is a generator	0 or 1	1

3. RESULTS AND DISCUSSIONS

To illustrate the efficacy of the established coherency identification process, the IEEE 30-Bus System, consisting of 6 generators, 24 load points, and 41 transmission lines, was employed. The dynamic simulation model of the IEEE 30-Bus System is obtained from an online repository [50].

The generators are assigned generator numbers so as to track their computation :

'Glen Lyn -1', 'Claytor -2', 'Fieldale -3', 'Reusens -4', 'Roanoke -5', 'Hancock -6'

These numbers would represent generators a & b to aid the implementation of the established coherency analysis scheme in the MATLAB environment. Thus, following the disturbance, the rotor angle and rotor speed data are captured and exported to MATLAB, where the formulated coherency grouping methodology is implemented. The results are further used with the minimal generation-load imbalance constraint to establish tie lines to open to form controlled islands back in the Powerworld simulator.

The synchronous generators are set to trip 2 seconds after over-frequency values of 1.04pu (62Hz) and under-frequency values of 0.96pu (57.6Hz) are reached. A steady-state simulation of the case study was carried out in Powerworld Simulator to obtain the MW output of generators. The MW output of the generators was further reduced by 35.6% (168MW) to enable the integration of inverter-based resources represented with the symbol of a wind turbine, all of the same capacity (168MW), on the following 132kV buses: Kumis, Hancock (II), Roanoke (II), and Blaine. This is achieved by integrating inverter-based resources of 42MW on each of the listed buses. In this way, a Renewable Energy Penetration Level (RPL) of 35.6% is achieved, as shown in Table 3.

Table 3: Grid-connected inverter-based resources on the IEEE 30-Bus System

Energy Sources	Bus Number	Bus Name	MW
Synchronous generators	1	Glen Lyn	198.3
	2	Claytor	38.6
	5	Fieldale	23.8
	8	Reusens	13.8
	11	Roanoke	12.4
	13	Hancock	17.3
Grid-connected inverter-based resources (35.6% RPL)	3	Kumis	42.0
	4	Hancock (II)	42.0
	6	Roanoke (II)	42.0
	7	Blaine	42.0
		Total MW	472.3

The implemented renewable energy-integration scheme is illustrated in Figure 2, with inverter-based renewables being represented by the wind turbine.

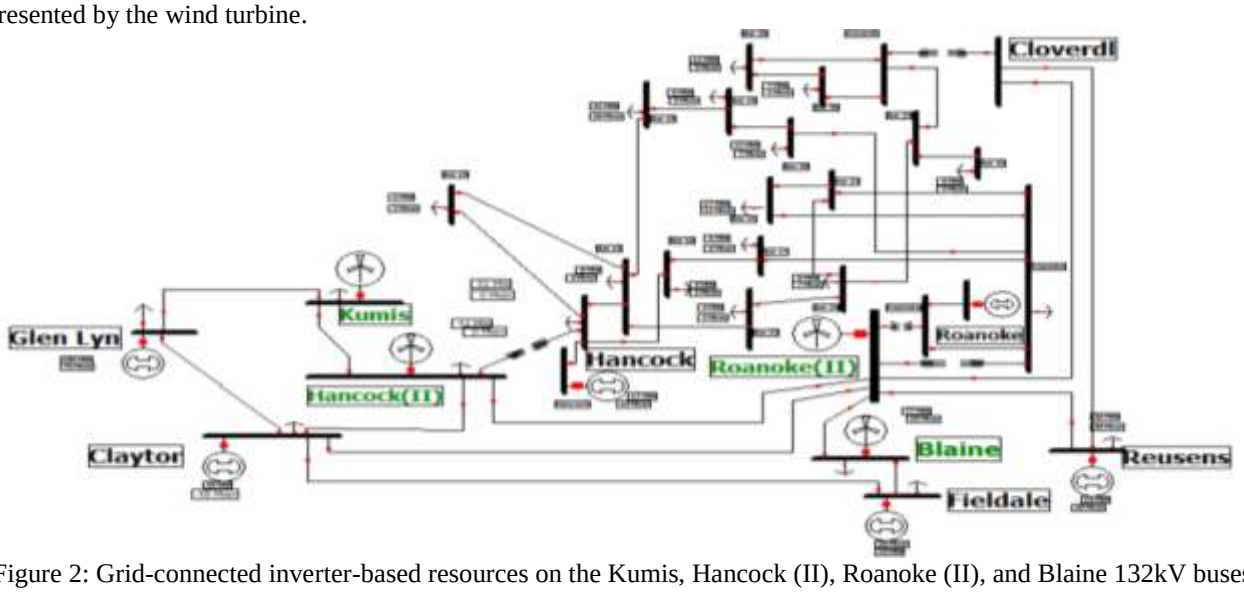

Figure 2: Grid-connected inverter-based resources on the Kumis, Hancock (II), Roanoke (II), and Blaine 132kV buses of the IEEE 30 bus-system

Thus, 3 scenarios are presented for this paper: 2 from the case study without inverter-based resources and 2 for the grid-connected inverter-based resources, as shown in Table 4:

Table 4: 3 scenarios presented

Scenario	Selected lines for 3-phase bolted fault	Situation Awareness	Fault Duration
1	Fieldale-Blaine & Reusens-Roanoke (II)	WITH grid-connected inverter-based resources (RPL of 35.6%)	4-7secs
2	Roanoke (II)-Claytor & Roanoke (II)-Blaine	WITHOUT grid-connected inverter-based renewables	4-7secs
3	Claytor-Fieldale and Claytor-Hancock (II)	WITH grid-connected inverter-based resources (RPL of 35.6%)	4-5secs

4.1 Scenario 1:

With the 42MW grid-connected inverter-based resources on the 132kV buses: Kumis, Hancock (II), Roanoke (II), and Blaine, the simulation begins for this scenario at steady state, after which the 132kV lines: Fieldale-Blaine & Reusens-Roanoke (II) are subjected to a 3-phase bolted fault at 4 secs and cleared at 7secs. The fault simulated is seen to propagate low-frequency disturbances on the rotor speeds and distortions from the inverter-based renewables shown in Figure 3.

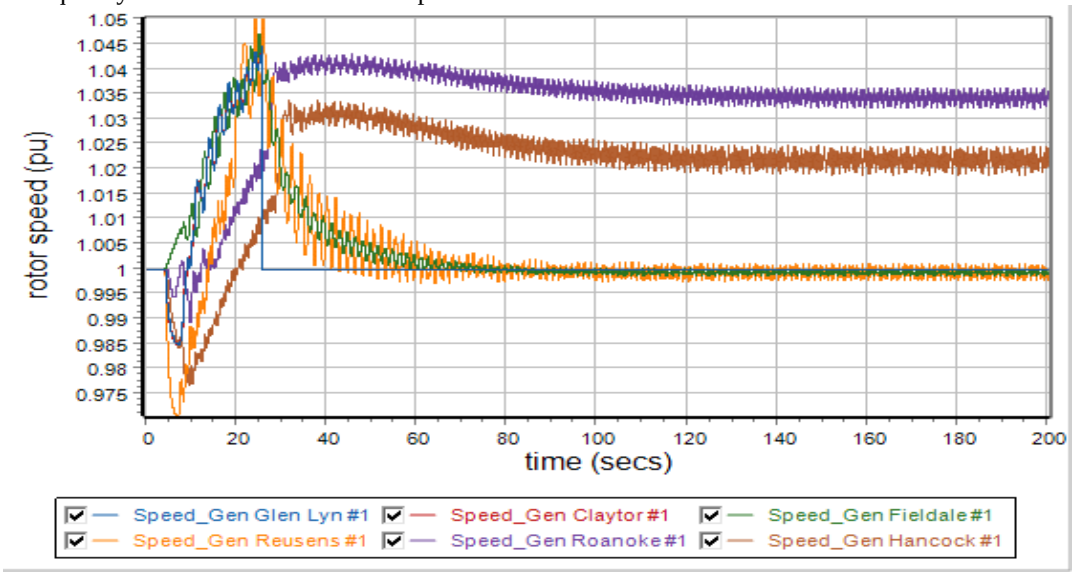

Figure 3: Rotor speed (pu) for scenario 1

Figure 4 also shows that the simulated 3-phase bolted fault on the Fieldale-Blaine & Reusens-Roanoke (II) 132kV lines significantly produces extreme levels of disturbances and low-frequency oscillations, and distortions from the inverter-based renewables on the system's bus voltage for the case study with grid-connect inverter-based renewables.

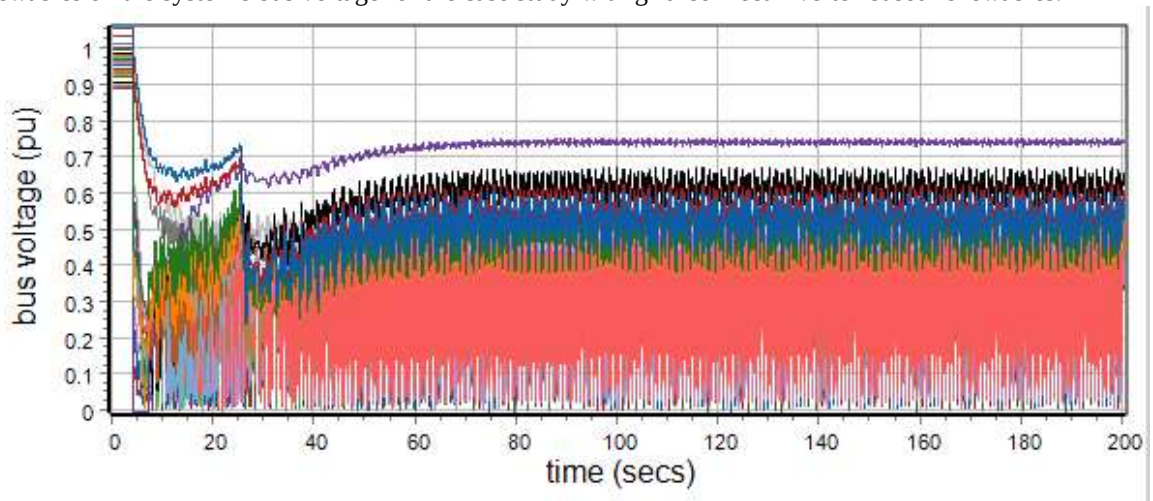

Figure 4: Bus voltage (pu) for scenario 1

With extreme disturbances on the power systems variable as well as a departure from their steady state, rotor angles, rotor speeds, and voltage instability can be said to be prevalent for this scenario. Scenario 1 is therefore suitable to implement the proposed coherency identification scheme. The rotor angles and rotor speeds for this scenario are collected between 10 and 11 seconds, after which the collected data were used to form the coherency results in Table 5.

Recall the numbers assigned to the generators:
'Glen Lyn -1', 'Claytor -2', 'Fieldale -3', 'Reusens -4', 'Roanoke -5', 'Hancock -6'

Furthermore, the adaptive coherency threshold $\gamma(t)$ was calculated to be 0.5321. The formulated Euclidean distance measures from rotor angles and rotor speed as shown in Table 5.

Table 5: Coherency results from distinct pair entries of the generators for scenario 1

$\delta_{norm}^{a,b}$	$\omega_{norm}^{a,b}$	$\lvert G^a \nabla G^b \rvert_{norm}$	a	b	$\lvert G^a \nabla G^b \rvert_{norm} < \gamma(t)$
0.004446	0.020217	0.0207	2	1	True
0.430351	0.175939	0.464926	3	1	True
0.434797	0.167145	0.465817	3	2	True
0.569649	0.775733	0.962425	4	1	FALSE!
0.565203	0.775344	0.959485	4	2	FALSE!
1	0.676725	1.207459	4	3	FALSE!
0.075092	0.493739	0.499417	5	1	True
0.078478	0.49335	0.499553	5	2	True
0.357982	0.394732	0.532883	5	3	FALSE!
0.642018	0.281993	0.701218	5	4	FALSE!
0.349676	1	1.059374	6	1	FALSE!
0.34523	0.999611	1.057547	6	2	FALSE!
0.780027	0.900993	1.191734	6	3	FALSE!
0.219973	0.224267	0.31414	6	4	True
0.422045	0.506261	0.659107	6	5	FALSE!

$|G^a \nabla G^b|_{norm}$ represents the normalized Euclidean distance of the formulated dynamic vector between generators a and b. For instance, the first row represents the Euclidean distance between the formulated vectors of generators 2 (Claytor) and 1(Glen Lyn), i.e., ($|G^2 \nabla G^1|_{norm}$) from Table 4, is less than the computed adaptive coherency threshold γ(t). Thus, generators 1(Glen Lyn) and 2 are coherent with each other. Similarly, the second row shows that generators 3 (Fieldale) and generator 1 (Glen Lyn), i.e., ($|G^3 \nabla G^1|_{norm}$) are coherent with each other from Table 5. The two entries considered have generator 1 (Glen Lyn) in common. Therefore, generators 1, 2, and 3, i.e., Glen Lyn, Claytor, and Fieldale, consequently belong to the same coherent group. In addition, going through the 1st to 15th entries of Table 5 shows that generator 6 (Hancock) and generator 4 (Reusens) are only coherent with themselves and should be placed in the same coherent group. Thus, in this way, by aggregating the coherent pairs $|G^a \nabla G^b|_{norm}$ which have one generator in common, groups of coherent generators are formed.

Table 6: Result of the coherency detection scheme for scenario 1

Generators	**Generator numbers**	**coherency results**	**Fault simulation period**	**Coherency Analysis Time Interval** $[T1 - T2]$
Glen Lyn	1	2,3,5	4-7secs on Fieldale-Blaine & Reusens-Roanoke 132kV lines	10-11secs
Claytor	2	1,3,5		
Fieldale	3	1,2	Coherency threshold ($\gamma(t)$)	0.5321
Reusens	4	6		
Roanoke	5	1,2		
Hancock	6	4		

Aggregating the generators that have one other generator in common concerning their coherency results produces 2 coherent groups:

Group 1; Hancock & Reusens
Group 2: Glen Lyn, Claytor, Fieldale, & Roanoke

Although the coherency analysis scheme proffers 2 coherent groups and consequently 2 controlled islands. It can be seen that the locations of Reusens & Hancock make it impractical to place them in the same coherent group due to their topological distance from each other as shown in Figure 5. Consequently, Reusens and Hancock are separated from each other. This therefore establishes why formed coherent groups should be validated with controlled islanding.

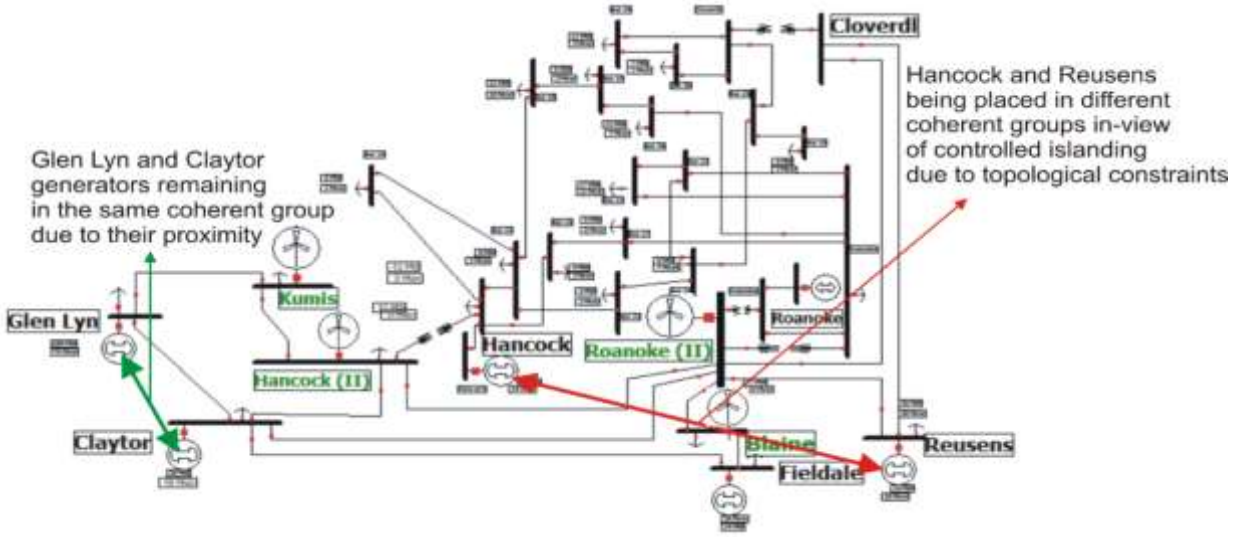

Figure 5: Impact of topological constraint on controlled islanding of scenario 1

Thus, by separating the Hancock and Reusens generators from each other, 3 coherent groups and consequently, 3 controlled islands are proposed to be energized as follows:
Island 1; Hancock
Island 2: Reusens
Island 3: Glen Lyn, Claytor, Fieldale, & Roanoke
By minimizing the generation-load imbalance as well as considerations based on topological constraints in regards to the load allocations to the respective islands using the Equation (12), the tie-lines to open to form the proposed islands, as illustrated in Figure 6, are: Reusens-Cloverdale and Reusens-Roanoke (II)132kV lines.

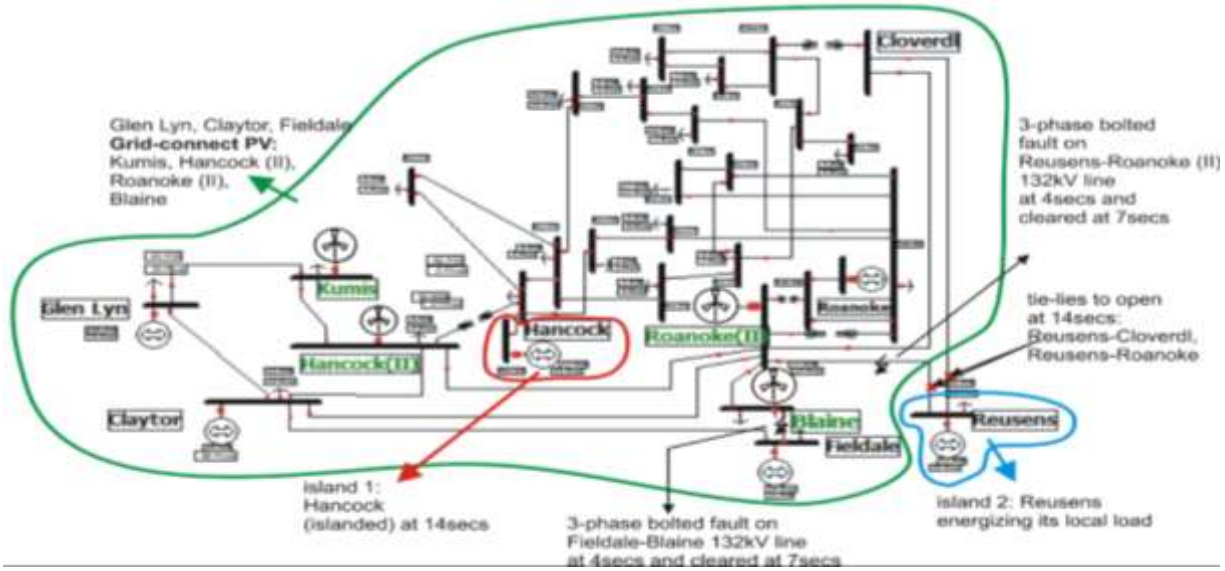

Figure 6: Proposed controlled islanding scheme for scenario 1

Table 7 further summarizes the load and generation allocated to each island in scenario 1, Hancock generated is islanded on its own without energizing any buses. Reusens generator is placed in the second island while Glen-Lyn, Claytor, Fieldale & Grid-connect inverter-based renewable are left to energize the third island.

Table 7: Proposed controlled islanding scheme for scenario 1

Generators for proposed islands (scenario 1)	**Total Generation per island (MW)**	**Load Buses Allocated**	**Total Load for proposed island (MW)**	**Tie-lines to open for island formation**
Island 1: Hancock	17MW	none	zero	Reusens-Cloverdale, Reusens-Roanoke (II), Hancock(generator)-Hancock
Island 2: Reusens	14MW	Reusens	30MW	Time for controlled islanding execution (*T_island*): 14secs
Island 3: Glen-Lyn, Claytor, Fieldale & Grid-connect INVERTER-BASED RENEWABLE	430.7MW	Fieldale, Glen Lyn, Hancock, Hancock (II), Bus 18, Kumis, Blaine, Bus 20, Claytor, Bus 21, Bus 29, Bus 19, Bus 17, Bus 24, Bus 15, Hancock, Bus 30, Bus 14, Roanoke, Roanoke (II), Bus 16, Bus 26, Bus 23	421.8MW	Loadshedding: None

The controlled islanding scheme implemented at 14 seconds is seen to dampen the disturbances on the rotor speed of the generators with 3 distinct rotor speed trajectories representing the rotor speed trajectories of the 3 islands, as illustrated in Figure 7:

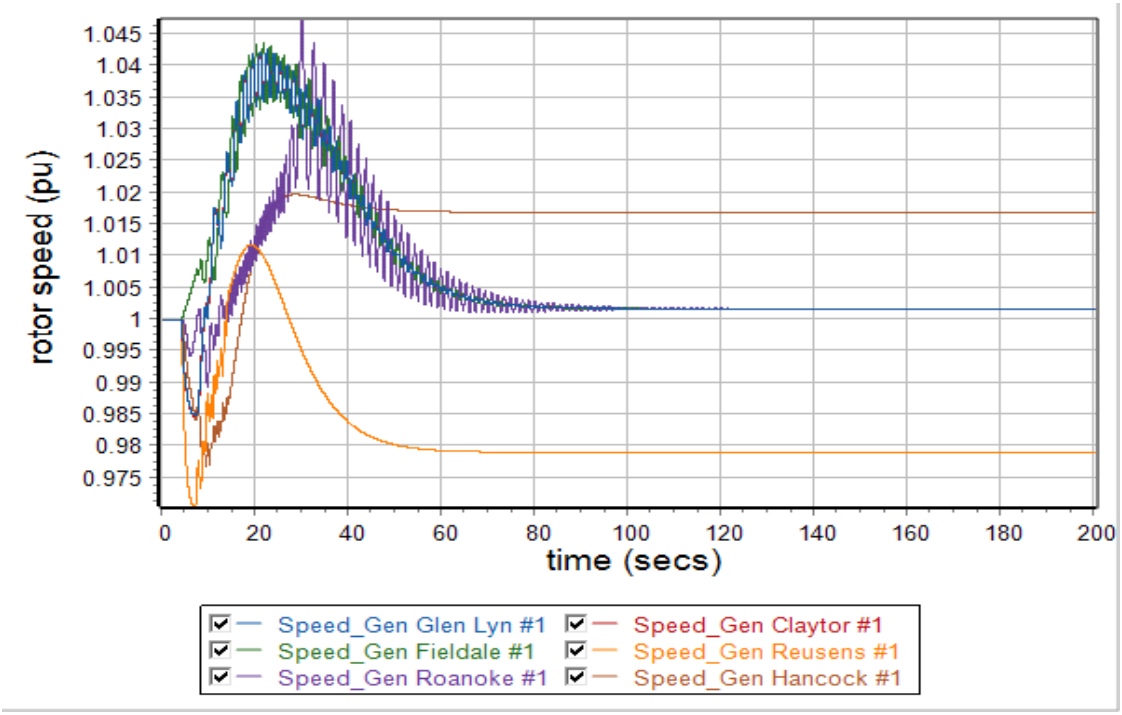

Figure 7: Rotor speed (pu) for scenario 1 after implementing coherency analysis and controlled islanding scheme at 14sec

It can also be seen from the figure that the disturbances on the system's bus voltage decay over time; thus, the efficacy of the established coherency and islanding scheme is illustrated in Figure 8

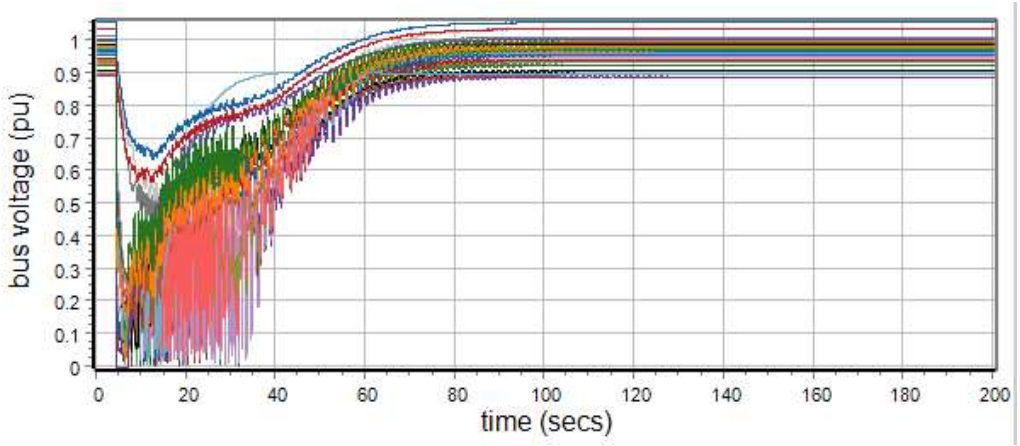

Figure 8: Bus voltage (pu) for scenario 1 after implementing coherency analysis and controlled islanding scheme at 14sec

4.2 Scenario 2:

This scenario does not contain any grid-connected inverter-based renewables. The 132kV lines: Roanoke (II)-Claytor & Roanoke (II)-Blaine are subjected to a 3-phase bolted fault at 4 secs and cleared at 7secs. The simulated fault can be seen to produce extreme system disturbances on the rotor speeds, which causes the Fieldale, Claytor, and Glen Lyn generators to trip on over frequency at 26.92 seconds, 27.62 seconds, and 28.26 seconds, respectively. The tripping of the Fieldale, Claytor, and Glen Lyn generators on over frequency creates further generation-load imbalance, which propagates the prevailing system disturbances enough to cause all the other generators: Roanoke, Hancock, and Reusens to trip on under frequency at 41.72secs, 42.1secs & 42.42secs respectively, as illustrated in Figure 9.

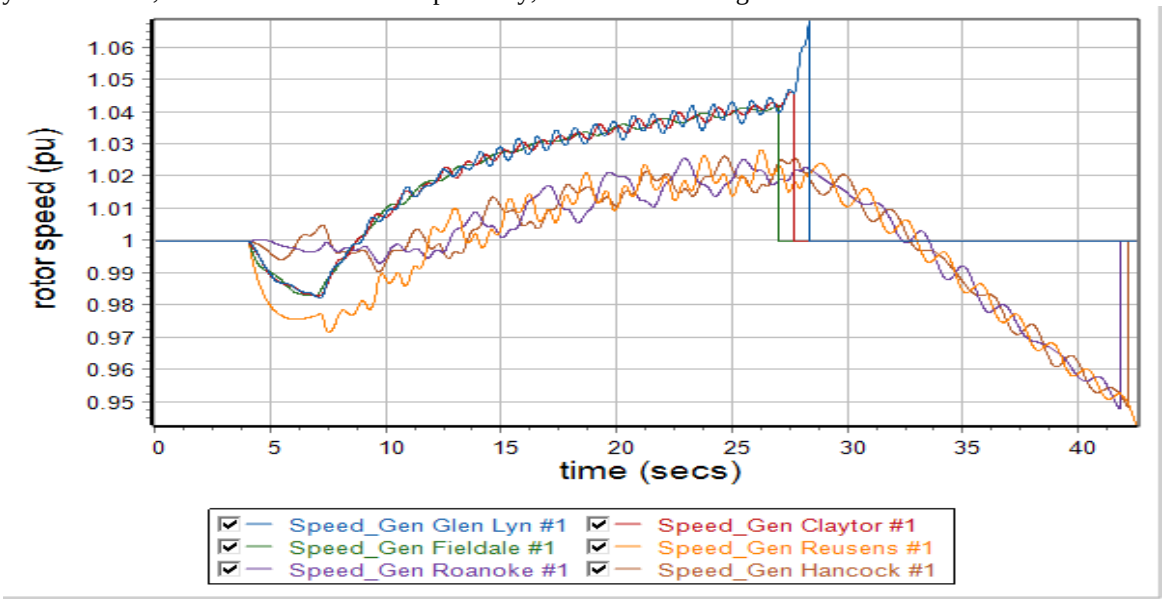

Figure 9: Rotor speed (pu) for Scenario 2

Figure 10 illustrates the effect of the propagated system disturbance on the bus voltages and imminent voltage collapse at 42.42 seconds as induced by the tripping of all the generators.

'Glen Lyn -1', 'Claytor -2', 'Fieldale -3', 'Reusens -4', 'Roanoke -5', 'Hancock -6'

With extreme disturbances and total voltage collapse established for scenario 2, the rotor angles and rotor speeds for this scenario are collected between 10 and 11.5 seconds, after which the collected data were used to form coherency results shown in Table 8 which evidently show from the 1st, 2nd and 3rd row that generator 2 (Claytor -2) and generator 1(Glen Lyn) are coherent, generator 3 (Fieldale) and generator 1(Glen Lyn) are coherent and Generator 3 (Fieldale) and generator 2 (Claytor) are coherent. The coherent pair in the 1st and 2nd entries has generators 1 in common and therefore should be placed in the same coherent group. In this way, generators 1,2, and 3 are placed in the same coherent group. Furthermore, going through the 4th to the 14th entries reveals that generator 4 (Reusens) is not coherent with any generator and therefore

is placed in its own separate coherent group away from the others. The 15th entry of Table 8, on the other hand, shows that generator 5 (Roanoke) and generator 6 (Hancock) should be placed in the same coherent group away from the other generators.

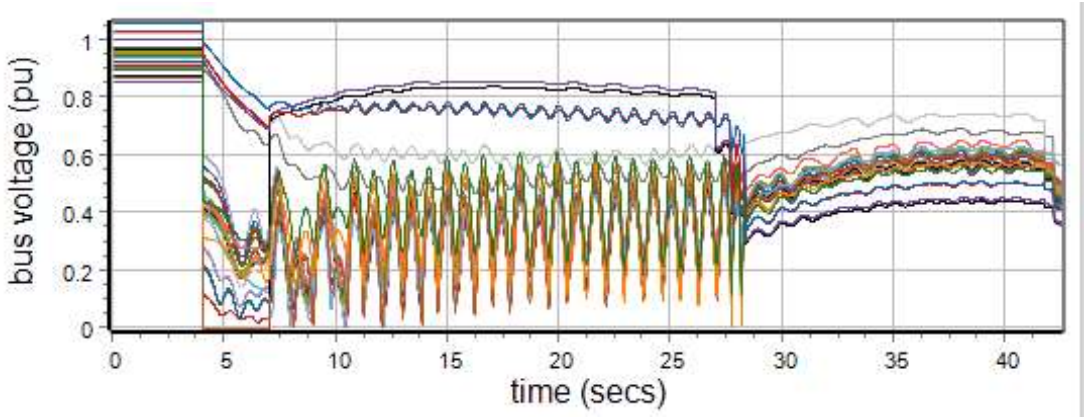

Figure 10: Bus voltage (pu) for Scenario 2

Table 8: Coherency results from distinct pair of generators for scenario 2

$\delta_{norm}^{a,b}$	$\omega_{norm}^{a,b}$	$\lvert G^a \nabla G^b \rvert_{norm}$	a	b	$\lvert G^a \nabla G^b \rvert_{norm} < \gamma(t)$
0.0104	0.0502	0.0512	2	1	True
0.0205	0.0779	0.0806	3	1	True
0.0100	0.0737	0.0744	3	2	True
0.7484	1.0000	1.2490	4	1	FALSE!
0.7380	0.9938	1.2378	4	2	FALSE!
0.7279	0.9798	1.2206	4	3	FALSE!
0.2516	0.5521	0.6067	5	1	FALSE!
0.2620	0.5459	0.6055	5	2	FALSE!
0.2721	0.5319	0.5974	5	3	FALSE!
1.0000	0.4479	1.0957	5	4	FALSE!
0.2438	0.6086	0.6556	6	1	FALSE!
0.2543	0.6024	0.6538	6	2	FALSE!
0.2643	0.5884	0.6450	6	3	FALSE!
0.9922	0.3914	1.0666	6	4	FALSE!
0.0110	0.0842	0.0849	6	5	True

The generator pairs in Table 8, which hold and have one generator in common, are clustered together to obtain the results summarized in Table 9

Table 9: Result of the coherency detection scheme for Scenario 2

Generators	**Generator numbers**	**coherency results**	**Fault simulation period**	**Coherency Analysis Time Interval** $[T1 - T2]$
Glen Lyn	1	1,2,3	4-7secs on Roanoke (II)-Claytor & Roanoke (II)-Blaine 132kV lines	10-11.5secs
Claytor	2	1,2,3	Coherency threshold (γ)	0.5917
Fieldale	3	1,2,3		
Reusens	4	4		
Roanoke (II)	5	5,6		
Hancock	6	5,6		

Aggregating the generators that have one generator in common to produce 3 coherent groups:
Group 1: Glen Lyn, Claytor, Fieldale
Group 2: Reusens
Group 3: Roanoke, Hancock

Evaluating the topological implications as well as the minimization generation-load using the Equation (12) establishes that the proposed controlled islanding establishes which opening of the following branches: Hancock-Hancock (II), Hancock (II)-Roanoke (II), Claytor-Roanoke (II), Roanoke (II)-Blaine, Reusens-Cloverdale & Reusens-Roanoke (II) as shown in Figure 11. Also, to minimize the generation-load imbalance in island 3, the load on the following buses is shed: Hancock, Bus 18, Bus 20 & Bus 21 as shown in Table 10:

Table 10: Table illustrating the proposed controlled islanding scheme for scenario 2

Coherent groups (Scenario 2)	**Total Generation per island (MW)**	**Load Buses Allocated**	**Total Load for proposed island (MW)**	**Tie-lines to open for island formation**
Island 1: Glen Lyn, Claytor, Fieldale	404.9MW	Glen Lyn, Claytor, Kumis, Hancock (II), Fieldale, Blaine	222.6MW	Hancock(b)-Hancock (II), Hancock (II)-Roanoke (II), Claytor-Roanoke (II), Roanoke (II)-Blaine, Reusens-Cloverdale & Reusens-Roanoke (II).
Island 2: Reusens	14MW	Reusens	30MW	Time for controlled islanding execution (*T_island*): 14secs
Island 3: Roanoke, Hancock	46.1MW	Bus 29, Bus 19, Bus 17, Bus 24, Bus 15, Hancock, Bus 30, Bus 14, Roanoke, Bus 16, Bus 26, Bus 23	76.6MW	Buses scheduled for loadshedding: Hancock, Bus 18, Bus 20, Bus 21 (122.6MW)

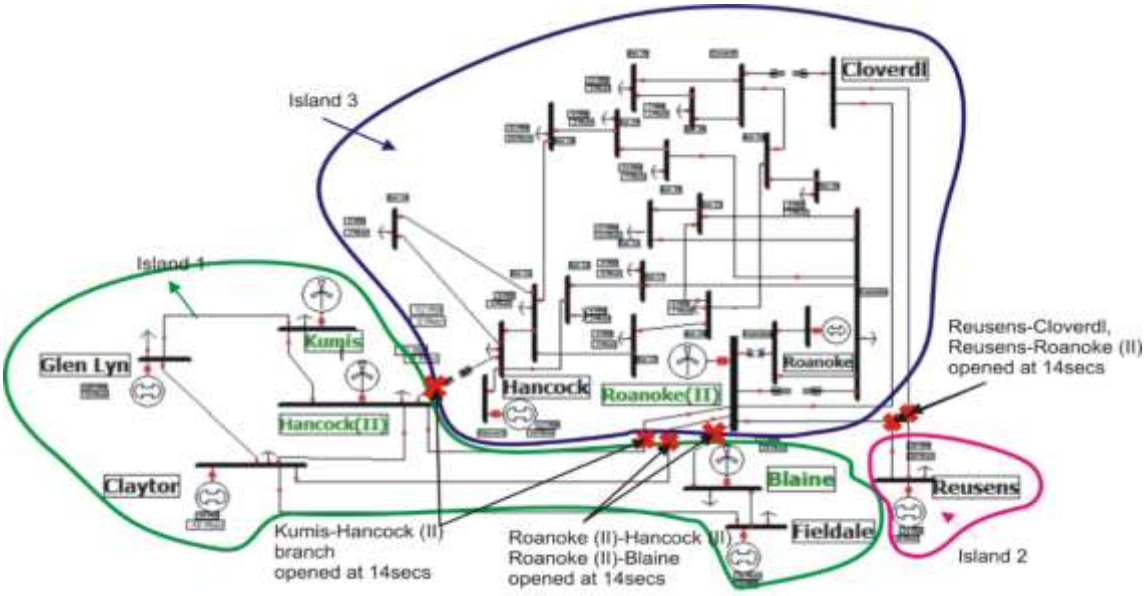

Figure 11: Illustration of the proposed islanding scheme for scenario 2

The controlled islanding scheme implemented at 14 seconds is seen to dampen the disturbances on the rotor speed of the generators, as illustrated in Figure 12.

The implemented coherency identification and controlled islanding scheme can also be seen to arrest the disturbances on the system's bus voltage decays over time, as shown in Figure 13

4.3 Scenario 3:

With the 42MW grid-connected inverter-based resources on the 132kV buses: Kumis, Hancock (II), Roanoke (II), and Blaine, the simulation for scenario 3 commences at steady state, after which the 132kV lines: Claytor-Fieldale & Claytor-Hancock (II) are subjected to a 3-phase bolted fault at 4 secs and cleared at 5secs.

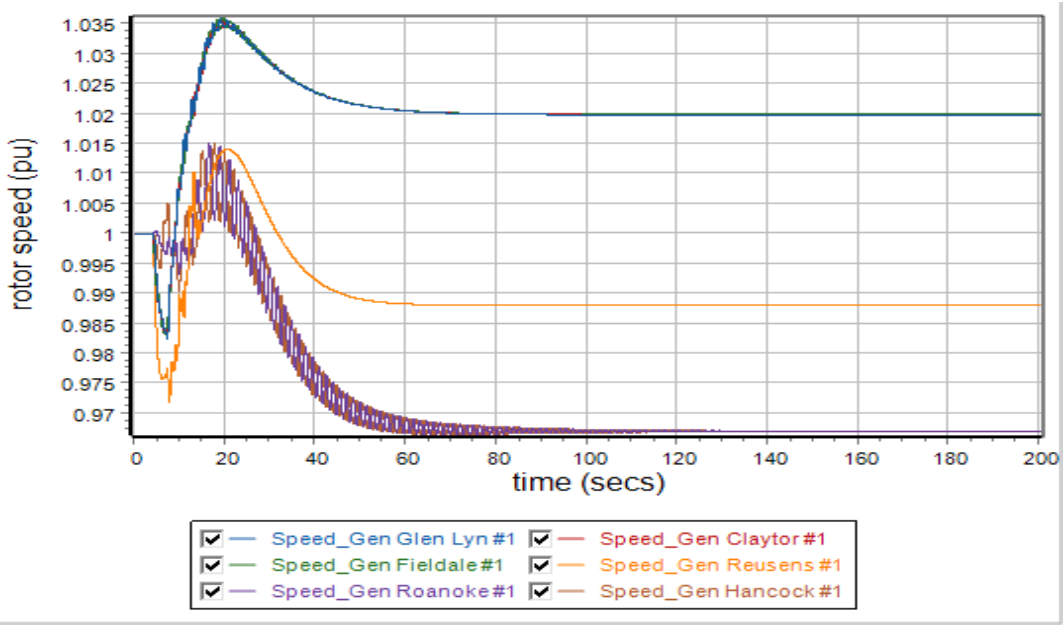

Figure 12: Rotor speed (pu) for scenario 2 after implementing coherency analysis and controlled islanding scheme at 14sec

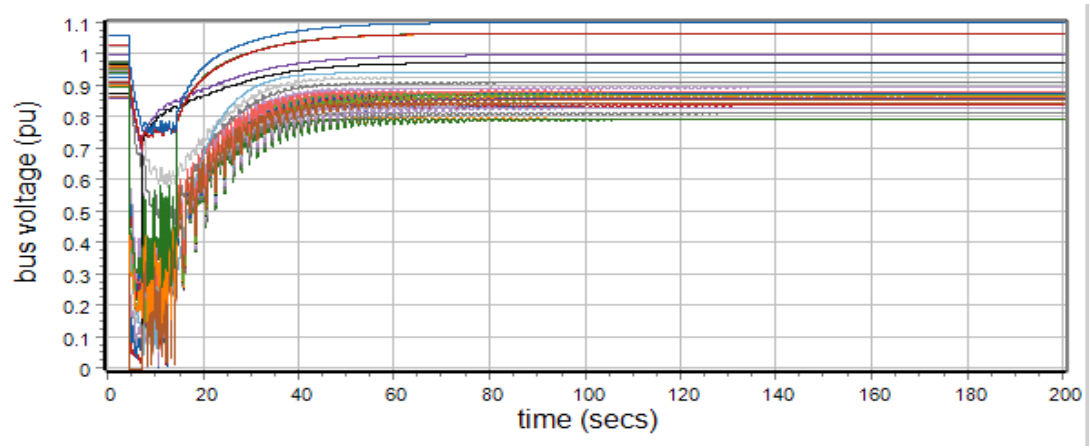

Figure 13: Bus voltage (pu) for scenario 2 after implementing coherency analysis and controlled islanding scheme at 14sec

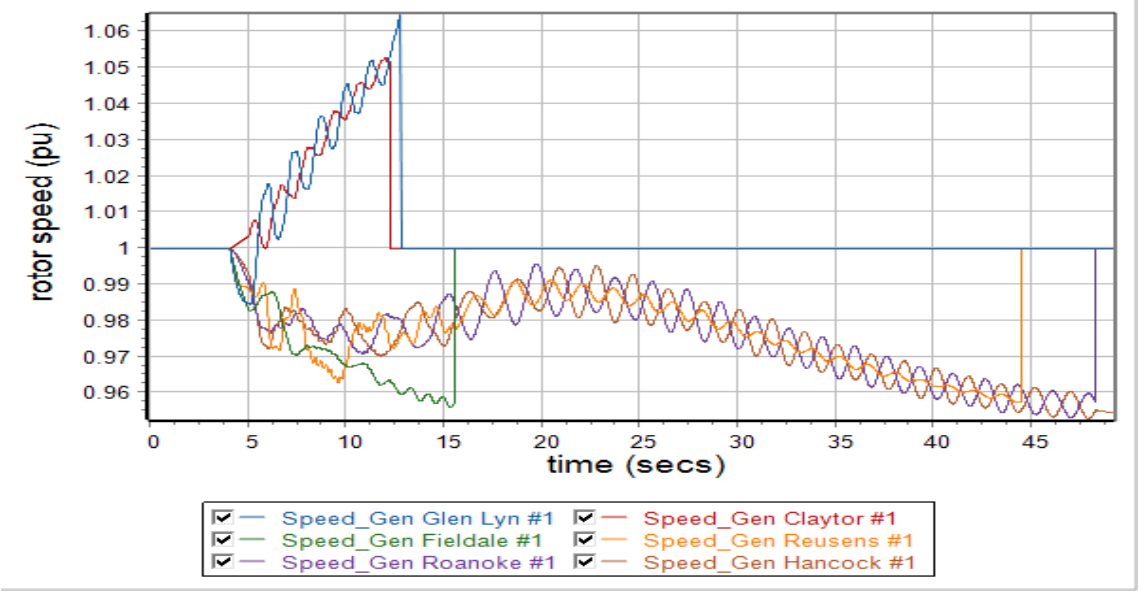

Figure 14: Rotor speed (pu) for scenario 3

The fault simulated is seen to induce system disturbances on the rotor speeds as well as cause a total voltage collapse due to the tripping of all the synchronous generators on various over-frequency and under-frequency violations, as shown in Figure 14.

A closer look at Figure 14 between 11 to 16 seconds reveals the tripping of the Claytor and Glen Lyn generators on over frequency at 12.22 and 12.72 seconds, respectively. The Fieldale generator can also be seen to trip on under frequency at 15.48 seconds, which further impacts the frequency stability of the renewable energy integrated power grid. The Reusens, Roanoke, and Hancock generators can also be seen to trip on under frequency at 44.4seconds, 48.22 seconds, and 49.08 seconds, leading to a voltage collapse as shown in Figure 15

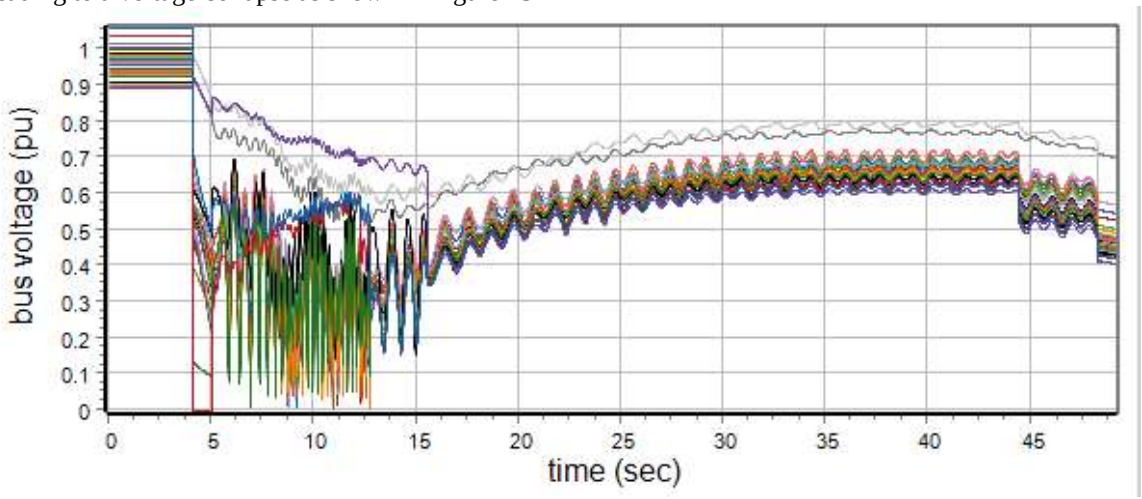

Figure 15: Bus voltage (pu) for scenario 3

Scenario 3 is therefore suitable to implement the unified coherency identification framework. The rotor angles and rotor speeds for this scenario are collected between 7 and to 8seconds, after which the collected data were used to form the coherency results shown in Table 11.

Table 11: Coherency results from distinct pairs of generators for scenario 3

$\delta_{norm}^{a,b}$	$\omega_{norm}^{a,b}$	$\lvert G^a \nabla G^b \rvert_{norm}$	a	b	$\lvert G^a \nabla G^b \rvert_{norm} < \gamma(t)$
0.174619	0.169126	0.243096	2	1	True
0.825381	1	1.296631	3	1	FALSE!
1	0.949255	1.378798	3	2	FALSE!
0.798343	0.800059	1.130241	4	1	FALSE!
0.972962	0.749314	1.228058	4	2	FALSE!
0.044989	0.204311	0.209205	4	3	True
0.804871	0.804625	1.138085	5	1	FALSE!
0.97949	0.75388	1.236016	5	2	FALSE!
0.035737	0.195375	0.198617	5	3	True
0.010777	0.096444	0.097044	5	4	True
0.799467	0.823145	1.147482	6	1	FALSE!
0.974087	0.7724	1.24316	6	2	FALSE!
0.036415	0.176855	0.180565	6	3	True
0.009052	0.06643	0.067044	6	4	True
0.007318	0.05224	0.05275	6	5	True

The coherent pairs $|G^a \nabla G^b|_{norm} < \gamma(t)$, which hold and have one generator in common, are clustered together to obtain the results in Table 12.

Aggregating the generator pairs that have one other generator in common concerning their coherency results produces 2 coherent groups.

Table 12: Result of the coherency detection scheme for scenario 3

Generators	**Generator numbers**	**coherency results**	**Fault simulation period**	**Coherency Analysis Time Interval $[T1 - T2]$**
Glen Lyn	1	1,2	4-5secs on Claytor-Fieldale & Claytor-Hancock (II)	7-8secs
Claytor	2	1,2		
Fieldale	3	3,4,5,6		
Reusens	4	3,4,5,6	Coherency threshold ($\gamma(t)$)	0.8701
Roanoke	5	3,4,5,6		
Hancock	6	3,4,5,6		

Group 1: Glen Lyn, Claytor
Group 2: Hancock, Reusens, Fieldale, & Roanoke

By minimizing the generation-load imbalance as well as considerations based on topological constraints in regards to the load allocations to the respective islands, the branches to open to form the proposed islands are on the proposed island are: Claytor-Roanoke (II), Claytor-Fieldale, Roanoke (II)-Hancock (II) and Hancock-Hancock (II) as shown in Table 13 and Figure 16.

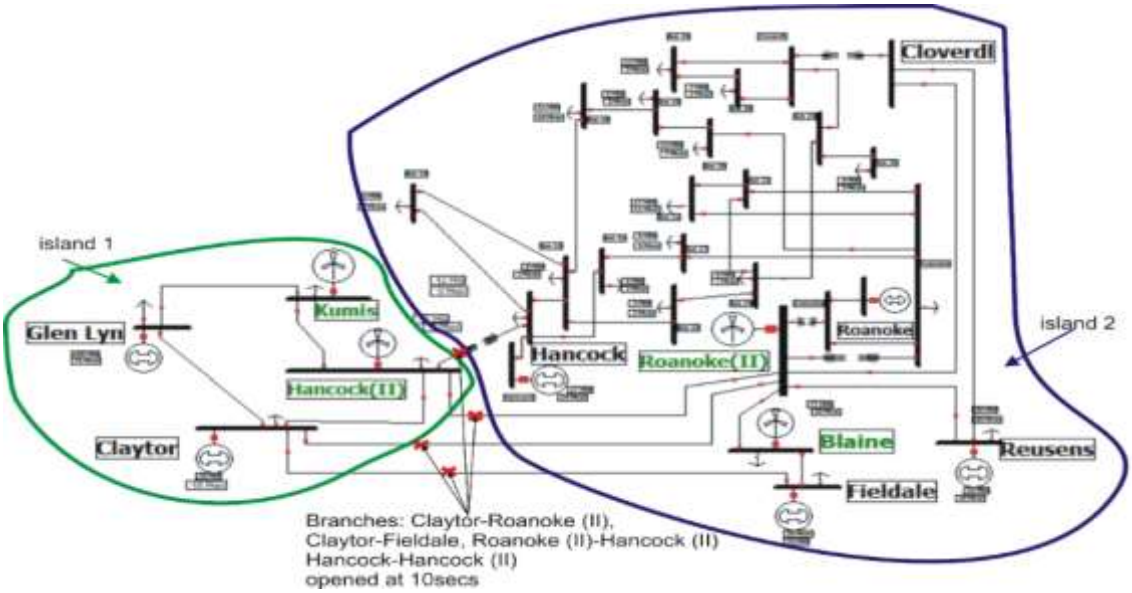

Figure 16: Proposed controlled islanding scheme for scenario 3

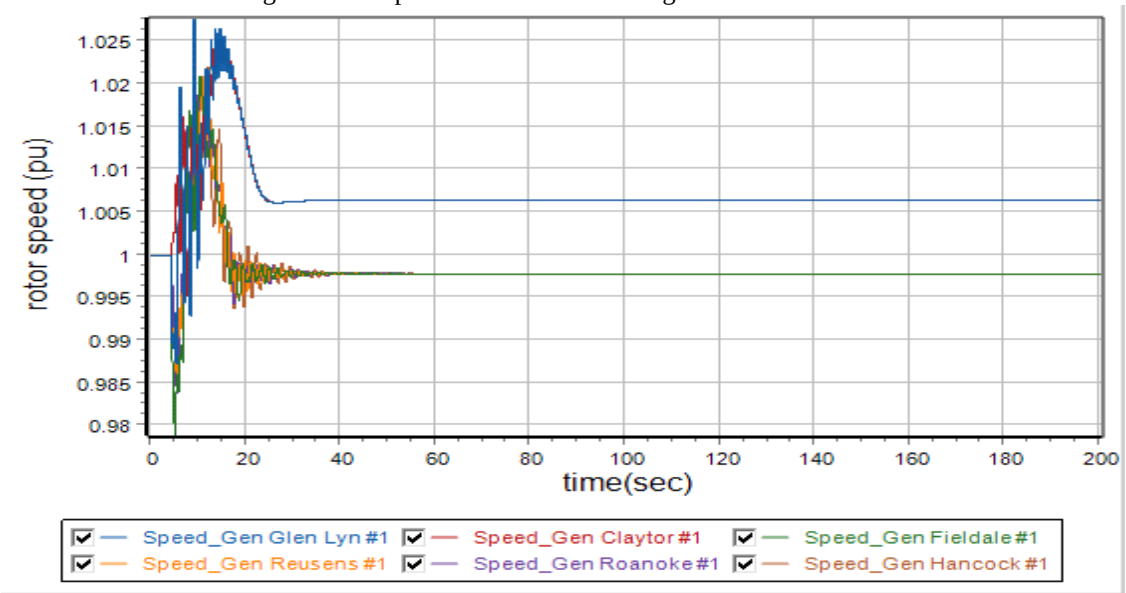

Figure 17: Rotor speed (pu) for scenario 3 after implementing the coherency analysis and controlled islanding scheme at 10 seconds.

The controlled islanding scheme implemented at 10 seconds is seen to dampen the disturbances on the rotor speed of the generators, as illustrated in Figure 17. It can also be seen from the figure that the disturbances on the system's bus voltage decay over time; thus, the efficacy of the established coherency and islanding scheme is illustrated in Figure 18.

Table 13: Proposed controlled islanding scheme for scenario 3

Coherent groups (scenario 3)	**Total Generation per island (MW)**	**Load Buses Allocated**	**Total Load for proposed island (MW)**	**Tie-lines to open for island formation**
Island 1: Glen Lyn, Claytor	226.6MW	Glen Lyn, Hancock (II), Kumis, Claytor,	122.4MW	Claytor-Roanoke (II), Claytor-Fieldale, Roanoke (II)-Hancock (II) Hancock-Hancock (II)
Island 2: Hancock, Reusens, Fieldale, Roanoke & Grid-connect INVERTER-BASED RENEWABLE:	235.6MW	Fieldale, Hancock, Bus 18, Blaine, Bus 20, Bus 21, Bus 29, Bus 19, Bus 17, Bus 24, Bus 15, Bus 30, Bus 14, Roanoke, Roanoke (II), Bus 16, Bus 26, Bus 23	299.4MW	Time for controlled islanding execution (*T_island*): 10secs Loadshedding: None

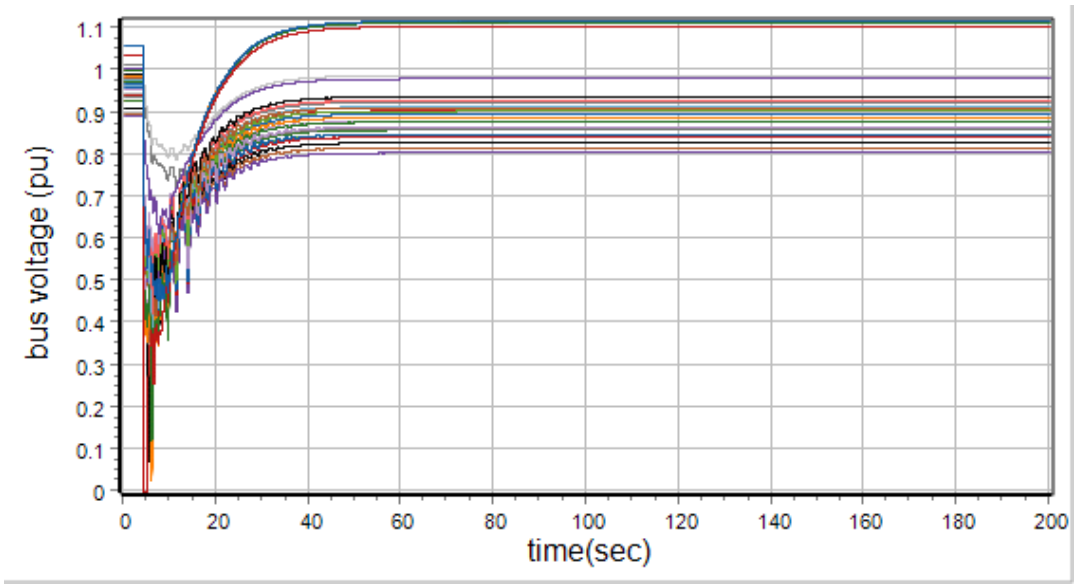

Figure 18: Bus voltage (pu) for scenario 3 after implementing coherency analysis and controlled islanding scheme at 10 seconds

The rotor angle trajectories can also be seen to illustrate the efficacy of the implemented coherency detection and controlled island scheme for scenario 3 at 10 seconds:

4.4 Comparison of Research with Previous Works:

The proposed method does consider the rotor angle and rotor speed dynamics. Various clustering techniques implemented for coherency detection, such as Fuzz-C-Means (FCM) [39], and K-Harmonic means [17] require the number of coherent groups to be specified before their implementation. There is therefore no means of determining an optimal number of coherent groups, whereas the proffered scheme does not require a priori, and its solution can be seen to be validated through the implementation of controlled-islanding. Clustering techniques pose a computational challenge, particularly for larger power grids, as they are generally iterative. Also, none of these methods tested the efficacy of the identified coherent groups through the implementation of controlled islanding. Thus, every established coherency grouping methodology should further be validated with controlled-islanding, particularly with the rise of renewable energy penetration levels. Additionally, traditional clustering assumes static patterns, but generator coherency can change over

time during or after disturbances, particularly with the intermittent nature of renewables. Static clustering fails to adapt to these dynamic changes. Power system responses during large disturbances are nonlinear, but many clustering techniques assume linear relationships and may not perform well in high-dimensional nonlinear spaces. Table 14 further shows a comparative analysis of the devised method with the traditional clustering approach.

Table 14: Comparative analysis of the formulated coherency detection and controlled islanding scheme

Criteria	Traditional Clustering Techniques	Proposed Rotor Angle–Speed Fusion Method
Input Data	Typically uses either rotor angle or rotor speed time-series data separately.	Simultaneously fuses rotor angles and rotor speeds into a unified dynamic vector, capturing complete electromechanical behaviour.
Parameter Dependency	Requires predefining the number of coherent groups (k) and sometimes cluster centroids.	Does not require a predefined number of coherent groups; grouping emerges naturally from threshold comparison.
Coherency Criterion	Based on geometric or statistical clustering boundaries.	Based on an adaptive coherency threshold that varies with system dynamics.
Adaptability to Time-Varying Conditions	Limited, static clustering cannot adapt to real-time operating changes.	Highly adaptive; coherency threshold adjusts with system state variations in real time.
Computational Complexity	It can be high, especially for large systems (hierarchical or spectral methods).	Relatively low; simple vector-based comparison allows efficient real-time execution.
Sensitivity to Noise and Initialization	Sensitive to noise, data scaling, and initial conditions (e.g., k-means centroids).	More robust, since coherency decisions rely on dynamic relationships rather than statistical partitions.
Suitability for Renewable-Rich Systems	Performance degrades under fast inverter-based dynamics due to a lack of inertia representation.	Effectively captures low-inertia dynamics and renewable variability through combined angle–speed representation.
Output	Fixed clusters of coherent generators.	Adaptive coherency groups that evolve with system dynamics.

4. CONCLUSION

A simple but effective framework for detecting coherent generators and implementation of controlled islanding following an extreme system disturbance of a renewable energy integrated power grid capable of stalling a total voltage collapse has been illustrated in this paper. Rotor angles and rotor speeds after simulation of a 3-phase bolted fault are captured, after which the established framework is implemented to obtain a coherent group of generators without a priori knowledge. The established coherency analysis scheme is enhanced by considerations of possible topological constraints, which may impact the number of coherent groups. After this, controlled islanding based on the minimization of generation-load imbalance is implemented based on the solutions of the applied coherency detection framework. The highlight of this research entails showing the efficacy of the proffered coherency analysis threshold and framework in arresting the propagation of extreme disturbances for a power grid with high penetration levels of renewables. In comparison to other methods established by previous authors, the scheme does not require a priori knowledge for detecting coherent groups. The proffered scheme is also seen to require low computational burdens with an adaptive coherency threshold method. Simulations are conducted in Powerworld, after which the rotor angles and rotor speed time series data are exported to

MATLAB, where the computations and scripts to establish coherency are written. The effectiveness of the approach shows its suitability in solving the coherence identification problem for a much larger renewable energy integrated power grid.

5. RECOMMENDATION FOR FUTURE WORK

Future research should focus on applying machine learning and deep learning methods, such as LSTM networks, graph neural networks, and autoencoders, to capture nonlinear relationships in generator dynamics and identify coherent groups from real-time measurements. With increasing renewable penetration, traditional rotor-angle-based coherency approaches must evolve to incorporate synthetic inertia, frequency response, and voltage control characteristics of inverter-based generators. Additionally, instead of assuming fixed coherent groups, future approaches should employ time-varying coherency detection that updates dynamically based on system operating states and event severity. Research should also consider exploring coherency analysis across hybrid networks where AC and DC subsystems interact, and where coherency may exist among microgrid clusters rather than individual machines. As wide-area controls rely on communication infrastructure, future frameworks should consider latency, data loss, and cybersecurity impacts on coherency-based control and islanding schemes. Finally, there is a need for benchmark datasets, standard test cases, and evaluation metrics to compare the performance of coherency identification techniques across different system sizes and operating conditions.

REFERENCES

[1] Samuel, I. A., Katende, J., Awosope, C. O. A., & Awelewa, A. A. (2017). Prediction of voltage collapse in electrical power system networks using a new voltage stability index. *International Journal of Applied Engineering Research*, *12*(2), 190–199.

[2] N.N., L., & V.V., V. (2018). Research into the loss of synchronism in power systems due to disturbances based on an analysis of electromechanical waves. *Energy Systems Research*, *1*(2), 69–86. doi:10.25729/esr.2018.02.0008

[3] Esmaeilian, A., & Kezunovic, M. (2017). Prevention of power grid blackouts using intentional islanding scheme. *IEEE Transactions on Industry Applications*, *53*(1), 622–629. doi:10.1109/TIA.2016.2614772

[4] Demetriou, P., Kyriacou, A., Kyriakides, E., & Panayiotou, C. (2019). Intentional Controlled Islanding of Power Systems Equipped With Battery Energy Storage Systems. *2019 IEEE Milan PowerTech*, 1–6.

[5] Fernández-Porras, P., Panteli, M., & Quirós-Tortós, J. (2018). Intentional controlled islanding: When to island for power system blackout prevention. *IET Generation, Transmission and Distribution*, *12*(14), 3542–3549. doi:10.1049/iet-gtd.2017.1526

[6] Samson, A. A., Popoola, O., & Mbey, V. (2021). An alternative framework for implementing generator coherency prediction and islanding detection scheme considering critical contingency in an interconnected power grid. *International Journal of Applied Science and Engineering*, *19*(4), 1–12.

[7] Zare, H., Yaghobi, H., & Alinejad-Beromi, Y. (2018). Adaptive concept of controlled islanding in power systems for wide-area out-of-step prediction of synchronous generators based on adaptive tripping index. *IET Generation, Transmission and Distribution*, *12*(16), 3829–3836. doi:10.1049/iet-gtd.2018.0319

[8] Lin, Z., Wen, F., Zhao, J., & Xue, Y. (2016). Controlled islanding schemes for interconnected power systems based on coherent generator group identification and wide-area measurements. *Journal of Modern Power Systems and Clean Energy*, *4*(3), 440–453. doi:10.1007/s40565-016-0215-6

[9] Babaei, M., & Abu-Siada, A. (2023). Intentional Controlled Islanding Strategy for Wind Power Plant Integrated Systems. *Energies*, *16*(12). doi:10.3390/en16124572

[10] Lin, Z., Wen, F., Ding, Y., Xue, Y., Liu, S., Zhao, Y., & Yi, S. (2018). WAMS-Based coherency detection for situational awareness in power systems with renewables. *IEEE Transactions on Power Systems*, *33*(5), 5410–5426. doi:10.1109/TPWRS.2018.2820066

[11] R. Monteiro, M., F. Alvarenga, G., R. Rodrigues, Y., Zambroni de Souza, A. C., L. Lopes, B. I., C. Passaro, M., & Abdelaziz, M. (2020). Network partitioning in coherent areas of static voltage stability applied to security region enhancement. *International Journal of Electrical Power and Energy Systems*, *117*(August 2019), 105623. doi:10.1016/j.ijepes.2019.105623

[12] Banna, H. U., Yu, Z., Shi, D., Wang, Z., Su, D., Xu, C., … Solanki, J. M. (2019). Online coherence identification using dynamic time warping for controlled islanding. *Journal of Modern Power Systems and Clean Energy*, *7*(1), 38–54. doi:10.1007/s40565-018-0443-z

[13] Demetriou, P., Hadjidemetriou, L., Kyriacou, A., Kyriakides, E., & Panayiotou, C. (2015). Real-time identification of coherent generator groups. *2015 IEEE Eindhoven PowerTech, PowerTech 2015*. doi:10.1109/PTC.2015.7232619

[14] Aghamohammadi, M. R., & Tabandeh, S. M. (2016). A new approach for online coherency identification in power systems based on correlation characteristics of generators rotor oscillations. *International Journal of Electrical Power and Energy Systems*, *83*, 470–484. doi:10.1016/j.ijepes.2016.04.019

[15] Khalil, A. M., & Iravani, R. (2016). A Dynamic Coherency Identification Method Based on Frequency Deviation Signals. *IEEE Transactions on Power Systems*, *31*(3), 1779–1787. doi:10.1109/TPWRS.2015.2452212

[16] Liu, S., Lin, Z., Zhao, Y., Liu, Y., Ding, Y., Zhang, B., … White, S. E. (2020). Robust System Separation Strategy Considering Online Wide-Area Coherency Identification and Uncertainties of Renewable Energy Sources. *IEEE Transactions on Power Systems*, *35*(5), 3574–3587. doi:10.1109/TPWRS.2020.2971966

[17] Wei, Y., Arunagirinathan, P., Arzani, A., & Kumar Venayagamoorthy, G. (2019). Situational awareness of coherency behavior of synchronous generators in a power system with utility-scale photovoltaics. *Electric Power Systems Research*, *172*(July 2018), 38–49. doi:10.1016/j.epsr.2019.02.021

[18] Yadav, R., Pradhan, A. K., & Kamwa, I. (2019). A Spectrum Similarity Approach for Identifying Coherency Change Patterns in Power System Due to Variability in Renewable Generation. *IEEE Transactions on Power Systems*, *34*(5), 3769–3779. doi:10.1109/TPWRS.2019.2903848

[19] Jafarzadeh, S., Genc, I., & Nehorai, A. (2021). Real-time transient stability prediction and coherency identification in power systems using Koopman mode analysis. *Electric Power Systems Research*, *201*(March), 107565. doi:10.1016/j.epsr.2021.107565

[20] Raak, F., Susuki, Y., & Hikihara, T. (2015). Multi-Way Partitioning of Power Networks via Koopman Mode Analysis. *IFAC-PapersOnLine*, *48*(30), 421–426. doi:10.1016/j.ifacol.2015.12.415

[21] Siddiqui, S. A., Verma, K., Niazi, K. R., & Fozdar, M. (2016). Real-time identification of generator coherent groups through synchrophasor measurements and ANN. *12th IEEE International Conference Electronics, Energy, Environment, Communication, Computer, Control: (E3-C3), INDICON 2015*, 1–5. doi:10.1109/INDICON.2015.7443128

[22] Gupta, A. K., Verma, K., & Niazi, K. R. (2018). *Power system low frequency oscillations monitoring and Generator Coherency Determination in Real Time*. *IEEE Innovative Smart Grid Technologies - Asia (ISGTAsia)*.

[23] Isnaadh, A., & Lukose, J. (2023). Generator coherency identification using a deep learning technique. In *PROCEEDINGS OF 5TH INTERNATIONAL CONFERENCE ON SUSTAINABLE INNOVATION IN ENGINEERING AND TECHNOLOGY (SIET) 2023* (p. 020022). Kuala Lumpur, Malaysia: AIP Publishing. doi:10.1063/5.0229678

[24] Quirós Tortos, J., Valverde, G., Ding, L., & Terzija, V. (2011). Optimal placement of Phasor Measurement Units to Improve Parallel Power System Restoration. *IEEE PES Innovative Smart Grid Technologies Conference Europe*. doi:10.1109/ISGTEurope.2011.6162687

[25] Tortos, J. Q., & Terzija, V. (2012). Controlled islanding strategy considering power system restoration constraints. *IEEE Power and Energy Society General Meeting*, (September). doi:10.1109/PESGM.2012.6344599

[26] Wang, X., DIng, L., Ma, Z., Azizipanah-Abarghooee, R., & Terzija, V. (2021). Perturbation-Based Sensitivity Analysis of Slow Coherency with Variable Power System Inertia. *IEEE Transactions on Power Systems*, *36*(2), 1121–1129. doi:10.1109/TPWRS.2020.3020837

[27] Song, H., Wu, J., & Wu, L. (2012). Controlled islanding based on slow-coherency and KWP theory. *2012 IEEE Innovative Smart Grid Technologies - Asia, ISGT Asia 2012*, 1–6. doi:10.1109/ISGT-Asia.2012.6303096

[28] Yang, B., Vittal, V., Heydt, G. T., & Sen, A. (2007). A novel slow coherency based graph theoretic islanding strategy. *2007 IEEE Power Engineering Society General Meeting, PES*. doi:10.1109/PES.2007.386173

[29] Chow, J. H., & Sanchez-Gasca, J. J. (2019). *Power System Coherency and Model Reduction*. *Power System Modeling, Computation, and Control*. doi:10.1002/9781119546924.ch16

[30] Stadler, J., Renner, H., & Köck, K. (2014). An inter-area oscillation based approach for coherency identification in power systems. *Proceedings - 2014 Power Systems Computation Conference, PSCC 2014*. doi:10.1109/PSCC.2014.7038314

[31] Wilfert, H. H., Voigtländer, K., & Erlich, I. (2001). Dynamic coherency identification of generators using self-organising feature maps. *Control Engineering Practice*, *9*(7), 769–775. doi:10.1016/S0967-0661(01)00028-4

[32] Zhou, Z., Bai, X., Zhao, S. S., Li, Z., Xu, J., Li, X., & Zhao, W. (2008). A new islanding boundary searching approach based on slow coherency and graph theoretic. *Proceedings - 4th International Conference on Natural Computation, ICNC 2008*, *6*(978), 438–442. doi:10.1109/ICNC.2008.523

[33] Badeeb, O. M. A., & Hazza, G. A. W. (2004). Application of the slow coherency decomposition method to the Yemeni network. *International Journal of Electrical Engineering and Education*, *41*(1), 56–63. doi:10.7227/IJEEE.41.1.5

[34] Zhu, Y., Chen, Y., Li, L., Qi, D., Huang, J., & Song, X. (2025). A coherent generator group identification algorithm under extreme conditions. *Global Energy Interconnection*, *8*(1), 92–105. doi:10.1016/j.gloei.2025.01.002

[35] Song, H., Wu, J., & Wu, K. (2014). A wide-area measurement systems-based adaptive strategy for controlled islanding in bulk power systems. *Energies*, *7*(4), 2631–2657. doi:10.3390/en7042631

[36] Mariotto, L., Pinheiro, H., Cardoso, G., Morais, A. P., & Muraro, M. R. (2010). Power systems transient stability indices: An algorithm based on equivalent clusters of coherent generators. *IET Generation, Transmission and Distribution*, *4*(11), 1223–1235. doi:10.1049/iet-gtd.2009.0647

[37] Vahidnia, A., Ledwich, G., Palmer, E., & Ghosh, A. (2012). Generator coherency and area detection in large power systems. *IET Generation, Transmission and Distribution*, *6*(9), 874–883. doi:10.1049/iet-gtd.2012.0091

[38] Wang, M. H., & Chang, H. C. (1994). Novel Clustering Method for Coherency Identification Using an Artificial Neural Network. *IEEE Transactions on Power Systems*, *9*(4), 2056–2062. doi:10.1109/59.331469
[39] Davarikia, H., Znidi, F., Aghamohammadi, M. R., & Iqbal, K. (2016). Identification of coherent groups of generators based on synchronization coefficient. In *IEEE Power and Energy Society General Meeting* (Vol. 2016-Novem, pp. 6–10). Research gate. doi:10.1109/PESGM.2016.7741434
[40] Khaitan, S. K., & McCalley, J. D. (2013). VANTAGE: A Lyapunov exponents based technique for identification of coherent groups of generators in power systems. *Electric Power Systems Research*, *105*, 33–38. doi:10.1016/j.epsr.2013.07.004
[41] Ourari, M. L., Dessaint, L. A., & Do, V. Q. (2003). Coherency Approach for Dynamic Equivalents of Large Power Systems. *International Conference on Power Systems Transients – IPST 2003 in New Orleans, USA Coherency*, *2*(1), 1–6.
[42] Ali, M., Mork, B. A., Bohmann, L. J., & Brown, L. E. (2013). Detection of coherent groups of generators and the need for system separation using synchrophasor data. *Proceedings of the 2013 IEEE 7th International Power Engineering and Optimization Conference, PEOCO 2013*, (June), 7–12. doi:10.1109/PEOCO.2013.6564506
[43] Lin, Z., Wen, F., Zhao, J., & Xue, Y. (2016). Controlled islanding schemes for interconnected power systems based on coherent generator group identification and wide-area measurements. *Journal of Modern Power Systems and Clean Energy*, *4*(3), 440–453. doi:10.1007/s40565-016-0215-6
[44] Demetriou, P., Quirós-Tortós, J., & Kyriakides, E. (2019). When to Island for Blackout Prevention. *IEEE Systems Journal*, *13*(3), 3326–3336. doi:10.1109/JSYST.2018.2866937
[45] Tang, F., Jia, J., Chen, L., Zhu, Z., Liu, J., Liao, Q., & Liu, D. (2016). Two-stage controlled islanding strategy based on Stoer-Wagner and improved Dinic algorithms. *Journal of Modern Power Systems and Clean Energy*, *4*(3), 454–466. doi:10.1007/s40565-016-0206-7
[46] Sun, K., Zheng, D. Z., & Lu, Q. (2005). A simulation study of OBDD-based proper splitting strategies for power systems under consideration of transient stability. *IEEE Transactions on Power Systems*, *20*(1), 389–399. doi:10.1109/TPWRS.2004.841239
[47] North American Electric Reliability Corporation (NERC). (2023). *Reliability Guideline, Parameterization of the DER_A Model for Aggregate DER*. North American Electric Reliability Corporation (NERC).
[48] Subedi, S., Vasquez-Plaza, J. D., Andrade, F., Rekabdarkolaee, H. M., Fourney, R., Tonkoski, R., & Hansen, T. M. (2024). Aggregate data-driven dynamic modeling of active distribution networks with DERs for voltage stability studies. *IET Renewable Power Generation*, (July). doi:10.1049/rpg2.13063
[49] Electric Power Research Institute (EPRI). (2019). The New Aggregated Distributed Energy Resources (DER_A) Model for Transmission Planning Studies: 2019 Update, 35.
[50] IEEE 30-Bus System. (2025, October 21). Retrieved 21 October 2025, from https://electricgrids.engr.tamu.edu/electric-grid-test-cases/ieee-30-bus-system/